Hindawi Publishing Corporation
Journal of Nanomaterials
Volume 2013, Article ID 795652, 10 pages
http://dx.doi.org/10.1155/2013/795652

Research Article

Synthesis and Visible Photocatalytic Activities of Poly(aminobenzoic acid)/TiO_2 Nanocomposites

Puhong Wen and Xiaomei Wang

Department of Chemistry and Chemical Engineering, Baoji University of Arts and Science, 1 Gaoxin Road, Baoji, Shaanxi 721013, China

Correspondence should be addressed to Puhong Wen; wenpuhong@gmail.com

Received 4 July 2013; Revised 23 November 2013; Accepted 10 December 2013

Academic Editor: Vladimir Agabekov

Three kinds of polymers, poly(*p*-aminobenzoic acid) (PPA), poly(*m*-aminobenzoic acid) (PMA), and poly(*o*-aminobenzoic acid) (POA), were prepared by oxidizing *p*-, *m*-, and *o*-aminobenzoic acid with $(NH_4)_2S_2O_8$ in acidic solution, respectively. Poly(aminobenzoic acid)/TiO_2 nanocomposites PPA/TiO_2, PMA/TiO_2, and POA/TiO_2 were prepared by adsorption of PPA, PMA, and POA polymers on surface of TiO_2 nanocrystals ST01 and P25, respectively. The polymers and the poly(aminobenzoic acid)/TiO_2 nanocomposites were studied by FT-IR and UV-visible spectra, TG-DTA analysis, SEM observation, and measurements of isotherms and adsorption model of the polymers on TiO_2 nanocrystals. Furthermore, the visible photoelectrochemical and photocatalytic activities of these nanocomposites were investigated by the photocatalytic decomposition of water and methylene blue under visible irradiation. These nanocomposites have exhibited higher and different the abovementioned activities. This difference can be attributed to the influence of site of amino group in aminobenzoic acid.

1. Introduction

Among the various semiconductor photocatalysts, titanium dioxide is one of the most popular and promising materials, because it is stable in various solvents under photoirradiation, it is also available commercially, and it can induce various types of redox reactions [1]. The enhancement of photocatalytic activity is needed for applications of photocatalytic reactions. It is thus important to increase efficiencies absorbing and utilizing light energy. But TiO_2 photocatalyst can absorb only the UV light with a wavelength region of below 400 nm that is only about 4% energy in the solar spectrum. Recently, there have been several attempts to enhance visible photocatalytic activity of TiO_2, such as modification of TiO_2 band gap by inducing oxygen-vacancy [2], replacing oxygen site with nitrogen [3], substituting Ti site with Cr, Fe, or Yb [4, 5], and modification of TiO_2 by adsorbing organic dye molecules as sensitizer on the surface [6, 7]. To develop suitable sensitizer, some studies have been carried out on the synthesis of organic dyes [8–12]. Polyaniline (PANI), as a well-known conducting polymer, has attracted a considerable interest in recent years because of its good stability, electrical, electrochemical, and optical properties [13–15]. The polyaniline and its derivatives can be expected to be utilized as a new type of photocatalytic sensitizer, because they are *p*-type semiconducting material. Very recently, we reported synthesis of poly(*o*-aminobenzoic acid) (POA), adsorption of the polymer on TiO_2 nanocrystals, and the behavior as photocatalytic sensitizer in the photocatalytic reaction [16]. In this study, three chemical reagents *p*-aminobenzoic acid (PAB), *m*-aminobenzoic acid (MAB), and *o*-aminobenzoic acid (OAB) were selected as the starting monomer of the polymerization for comparing the activities of these polymers as photocatalytic sensitizer, because they have a carboxyl group located on the para-, meta-, or ortho-position of amino-group in the benzene ring, it will be polymerized into a poly (aminobenzoic acid) with straight-chain structure. In these polymers, the $-NH_2$ groups can be utilized in the polymerization reaction, and carboxyl groups can be used to combine to Ti(IV) on TiO_2 surface by a multi-bridging chelating coordination [16]. The synthesized poly(aminobenzoic acids) and the poly(aminobenzoic acid)/TiO_2 nanocomposites obtained by adsorption of the

polymer on TiO_2 nanocrystals were studied by FT-IR and UV-visible spectra, TG-DTA analysis, SEM observation, and measurements of isotherms and adsorption model of the polymers on TiO_2 nanocrystals. Furthermore, the visible photoelectrochemical and photocatalytic activities of these nanocomposites were investigated by the photocatalytic decomposition of water and methylene blue under visible irradiation. These nanocomposites have exhibited higher and different the above-mentioned activities. This difference can be attributed to the influence of site of amino group in aminobenzoic acid.

2. Experimental Details

2.1. Materials. ST01 (commercial TiO_2 powder, anatase phase, crystal size about 7 nm, BET surface area 349 $m^2 \cdot g^{-1}$) was obtained from Ishihara. P25 (commercial TiO_2 powder, mixed phases of anatase and rutile, crystal size about 30 nm, BET surface area 63 $m^2 \cdot g^{-1}$) was obtained from Degussa. N719 (*cis*-di(thiocyanate) bis(2,2′-bipyridyl-4,4′-dicarboxylate)-ruthenium(II) bis-tetrabutyl-ammonium) was purchased from Sigma-Aldrich. Other chemicals and reagents were of analytical grade, and all the reagents were used as received without further purification.

2.2. Synthesis of Poly(aminobenzoic acid). Poly(amin- obenzoic acid) was synthesized by oxidizing aminobenzoic acid with an oxidizing agent of peroxodisulfate ammonium $(NH_4)_2S_2O_8$ in an acidic solution. A mixed solution containing 0.1 mol/L *p*-aminobenzoic acid, 0.15 mol/L $(NH_4)_2S_2O_8$, and 0.2 mol/L HNO_3 was reacted at 40°C for 24 h with stirring. After the reaction, the precipitated solid was separated from the solution by centrifugation, then washed with distilled water, and finally dried at 40°C. The polymer poly(*p*-aminobenzoic acid) (PPA) is obtained. The synthesis methods of polymers poly(*m*-aminobenzoic acid) (PMA) and POA were similar to that of PPA. In the synthesis, the molar ratio of aminobenzoic acid/peroxodisulfate ammonium/nitric acid is selected as 1/3/1 for PMA and 1/1/3 for POA, respectively, for obtaining products with larger absorbance on visible light and pledging higher reacting speed.

2.3. Adsorption of Polymer on TiO_2 Nanocrystals. Ishihara ST01 and Degussa P25 were used as TiO_2 nanocrystal samples in adsorption experiments. The adsorption experiment of the polymer on TiO_2 nanocrystals was carried by a batch method. TiO_2 nanocrystal powder sample (5 mg) was added into an ethanol solution (5 mL) of the polymer in a concentration range of 0.06 to 0.5 $g \cdot L^{-1}$, and then stirred at room temperature for 72 h. After the adsorption, the liquid phase was separated from the solid phase by centrifugation, and then the concentration of the polymer in the solution was analyzed using SHIMADZU UV-2450 spectrophotometer. The solid phase was washed with ethanol for 3 times and dried at 40°C. The TiO_2 nanocrystal sample was calcined at 450°C for 30 min before using in the adsorption experiment [17]. A TiO_2 nanocrystalline film on conducting glass (FTO coated glass) was prepared by coating the conducting glass surface with ST01 or P25 TiO_2 nanocrystal paste and then calcined at 450°C for 60 min. A polymer/TiO_2 nanocomposite film was obtained by soaking the TiO_2 film in 0.3 $g \cdot L^{-1}$ polymer ethanol solution for 24 h.

2.4. Physical Analysis. FT-IR spectra of the samples were measured on a PERKIN ELMER SPECTRUM ONE spectrophotometer at a resolution of better than 2 cm^{-1} using the KBr technique. UV-visible spectra were recorded on a SHIMADZU UV-2450 spectrophotometer. Scanning electron microscopy (SEM) observation was performed on JEOL JSM-5500S. Nitrogen gas adsorption was carried out on a QUANTACHROME AUTOSORB-1-MP apparatus. The specific surface area was calculated from the adsorption data using the Brunauer-Emmett-Teller (BET) method. Simultaneous thermogravimetry and differential thermal analysis (TG-DTA) data were obtained on a SHIMADZU DTG-60H thermal analyzer at a heating rate of 10°C/min in air. In the photoelectrochemical and electrochemical measurements, a Hokuto-Denko BAS100B electrochemical analyzer was used.

2.5. Measurement of Photocatalytic Activity. The visible photocatalytic activity of polymer/TiO_2 nanocomposite was characterized by methylene blue (MB) degradation method and photoelectrochemical method. In the MB degradation method, the nanocomposite powder sample (30 mg) was added in the MB aqueous solution (150 mL, 5 ppm), and then irradiated with a 300 W, 110 V TAI incandescent lamp made by Toshiba Corp. in Japan located at 1 m from the MB solution. The spectral range of the lamp is mainly in visible range and containing about 5% UV-light. The concentration of MB in the solution was measured using SHIMADZU UV-2450 spectrophotometer. A blank experiment was carried simultaneously using 5 ppm MB solution without TiO_2 to deduct MB degradation by direct photoreaction. The amount of MB adsorbed on sample surface was evaluated by desorbing MB from the sample with a 0.1 mol/L HCl solution after photocatalytic degradation experiment. The decrease amount of MB by the adsorption was removed from the degradation amount by the photocatalytic reaction. A sample of polymer-free TiO_2 was used also as the reference in the visible photocatalytic active study.

In the photoelectrochemical measurement, the polymer/TiO_2 nanocomposite film was used as working electrode, and irradiated in a quartz cell containing sodium sulfate supporting electrolyte solution using a Xe lamp (Asahi Spectra USA LAX-Cute, VIS 400–700 nm) with a light intensity of 3000 W/m^2. The masked-off irradiated area was 1.13 cm^2. A Pt plate and an $Hg/Hg_2Cl_2/KCl_{sat}$ electrode were used as counter and reference electrodes respectively. An external bias was applied, and photocurrent was measured using the electrochemical analyzer.

3. Results and Discussion

3.1. Synthesis and Characterization of Poly(aminobenzoic acid). The polymers were synthesized by mixed the solutions

of aminobenzoic acid and peroxodisulfate ammonium. The aminobenzoic acid has an aromatic structure similar to aniline that can be polymerized to polyaniline by an oxidation reaction [18, 19]. The long conjugated system of polyaniline leads to absorption of visible light in a wide wavelength region and electric conduction. It is expected that aminobenzoic acids can be polymerized also to a poly(aminobenzoic acid). The mechanism of the polymerizing reaction is similar to that of aniline [14]. In the reaction, $(NH_4)_2S_2O_8$ is used as an oxidizing agent and the strongly acidic environment requiring for the reaction is provided by nitric acid. When $(NH_4)_2S_2O_8$ solution is added into the aminobenzoic acid solution, free radicals as initiating agent produced by breaking peroxodisulfate can attract the activated hydrogen of amino group of aminobenzoic acid, resulted new free radical of aminobenzoic acid molecular. The new free radical can attract aminobenzoic acid molecular, and then acted with the initiating agent free radical for completing a substitution reaction on the aromatic ring by free radicals. This substitution product can be attracted and lengthened further by free radical of aminobenzoic acid molecular. The product with enough great molecular weight can be precipitated from reacting solution. Therefore, polymerizations of lengthened chain can be ended, and formed PPA, PMA and POA respectively. The carboxyl groups on the poly(aminobenzoic acid) can be utilized for the adsorption of this polymer on TiO_2 surface similar to the case of ruthenium bipyridryl derivative dyes [20].

The optical absorption properties of synthesized polymers are dependent also on their synthesis conditions, such as the concentration of $(NH_4)_2S_2O_8$ oxidizing agent and HNO_3. The influences produced by amount of oxidizing agent and the acid are different in the synthesis of PPA, PMA, and POA because of the difference of site of amino group in aminobenzoic acid. The increase of amount of oxidizing agent is not advantage to enhance the visible light absorption of polymers PPA and POA, but is advantage for polymer PMA. The increase of HNO_3 concentration is advantage to enhance the visible light absorption of polymer POA, but lead to decrease greatly the visible light absorption of polymers PPA and PMA and color of the sample change to light.

A precipitate was formed by aminobenzoic acid reacted with $(NH_4)_2S_2O_8$ in acidic solution. Colors of precipitates are black for POA, brown for PPA, and brown-black for PMA, respectively. Their SEM images were shown in Figure 1. It is observed that their morphology show hollow ball-like for POA (Figure 1(a)), grain-like for PPA (Figure 1(b)) and branch-like for PMA (Figure 1(c)), respectively. The solubility of the polymer samples in water solvent is low, while it is high in ethanol solvent. The UV-visible absorption spectra of synthesized polymers and their monomers in ethanol solvent are shown in Figure 2. The absorption spectrum of N719 dye in ethanol solvent is also shown in Figure 2 for the comparison. It is observed that all monomer have not absorption in visible light range, while the polymer PPA, PMA, and POA reveal a broad absorption band between 400 and 700 nm. The correlating data are summarized in Table 1. Their absorption peaks red shift to 300 and 391 nm for PPA, 331 and 346 nm for PMA, and 350 and 550 nm for POA compared with their monomers. The absorbance coefficients of the polymers in visible light region are much larger than that of N719 dye used in dye-sensitized solar cell. The average value of absorbance coefficient in 400–600 nm increases in the order of N719 < PMA < PPA < POA. The results indicate that the conjugation extent and activity absorbing on visible light of the molecular chain increase in the order of PMA < PPA < POA because their monomers have a same molecular weight. The polyaniline also shows two absorption peaks around 360 and 600 nm in water solvent, which can be attributed to the π-π^* transition of the benzenoid rings and the exciton transition of the quinoid rings, respectively [21]. This fact indicated that the carboxylic acid groups substituted on the benzene rings cause a blue shift due to their electron-withdrawing nature [18].

Figure 3 showed the TG and DTA curves of the polymers. As shown in Figure 3, the decomposition of main part approaching 95% occurred at 200 to 650°C and formed broad exothermic peak corresponding to the burnout of the polymer. The broad peaks indicate they are a mixture with different polymeric degree. The results illustrate they are thermal stable polymers.

The FT-IR spectra of synthesized polymers and their monomers samples are shown in Figure 4. The correlating data are summarized in Table 1. It is found that the main differences between the IR spectra of the monomer and the polymer are vibration bands of the amino groups. The sharp ν(N–H) bands located at around 3500~3300 cm^{-1} of PAB and OAB changed to broad bands, and ν(C–N) band at around 1350~1325 cm^{-1} changed to a broad band and red shift, after the polymerization reaction. The two strong bands at 1692 and 1292 cm^{-1} for PPA and 1688 and 1247 cm^{-1} for POA are assigned to the ν(C=O) and ν(C–OH) group of carboxylic acid (–COOH). The two weak bands at 1579 and 1385 cm^{-1} for PPA and 1606 cm^{-1} and 1385 cm^{-1} for POA are assigned to the asymmetric ($-COO^-$as) and the symmetric ($-COO^-$s) stretches of the carboxylate group, respectively. It is observed the absence of character bands of asymmetric and symmetric stretch vibration (N–H) of aromatic primary amine and the presence of vibration bands of carboxylate group in the FT-IR of MAB [22]. It suggests hydrogen bands between primary amine group and carboxylic acid group exist in MAB. The spectrum of PMA showed the presence of carboxylic acid and carboxylate groups. The strong band at 1697 cm^{-1} is assigned to the ν(C=O) group of carboxylic acid. The shoulder band at 1610 cm^{-1} ($-COO^-$as) and medium band at 1385 cm^{-1} ($-COO^-$s) can be assigned to the asymmetric and the symmetric stretch of the carboxylate group, respectively. The broad band at 3416 and strong band at 1301 cm^{-1} are assigned to the ν(N–H) and ν(C–N) groups of aromatic secondary amine, respectively. The broad band at 3223 cm^{-1} and strong band at 1579 cm^{-1} are assigned to stretching vibration and bend vibration of N–H of NH_3^+ groups, respectively. These results reveal that amino groups are used for the polymerization reaction similar to the case of polyaniline, and carboxylic acid group was not used for the polymerization reaction since the bands of this group were remained after the polymerization reaction.

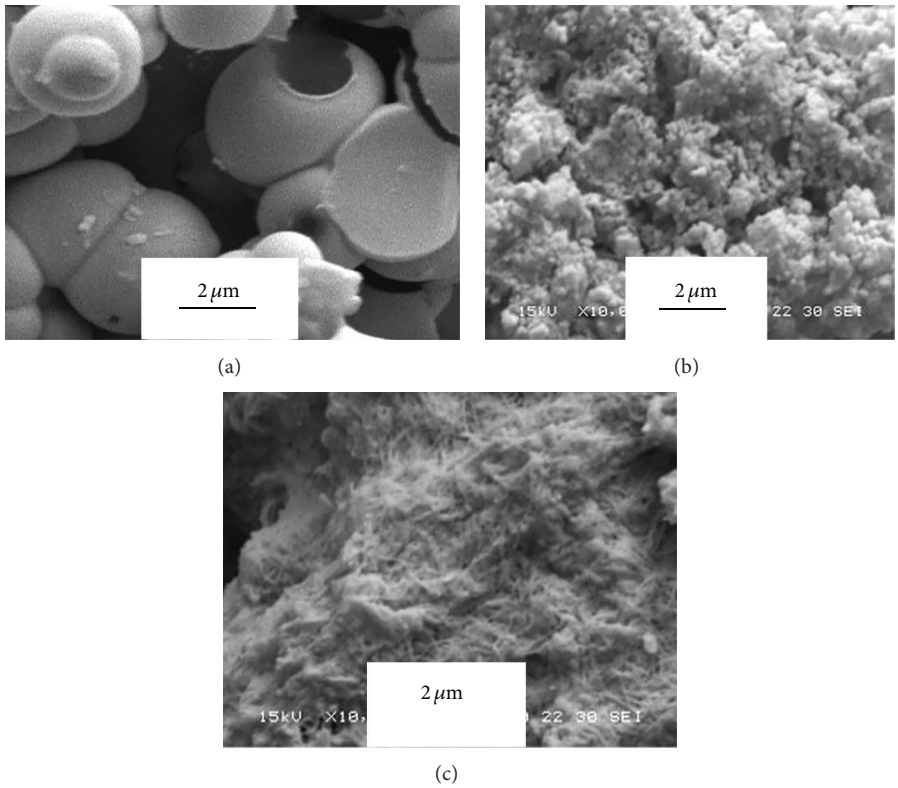

Figure 1: SEM images of samples (a) POA, (b) PPA, and (c) PMA.

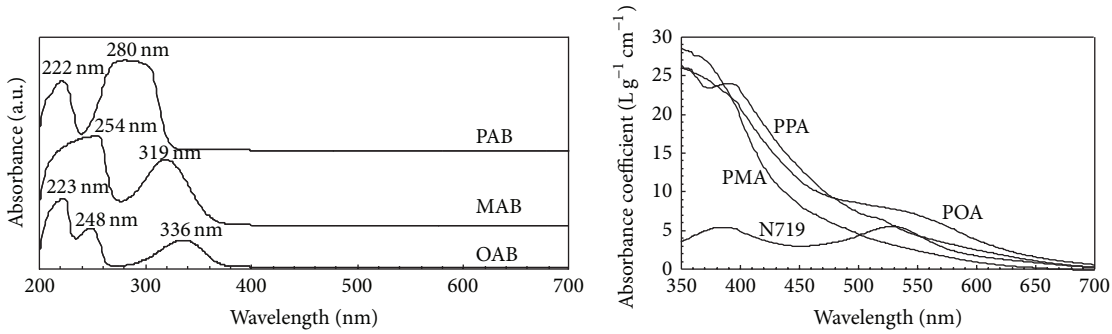

Figure 2: UV-visible spectra ofsamplesin ethanol. (a) PAB, MAB, and OAB monomer and (b) the polymers and dye N719.

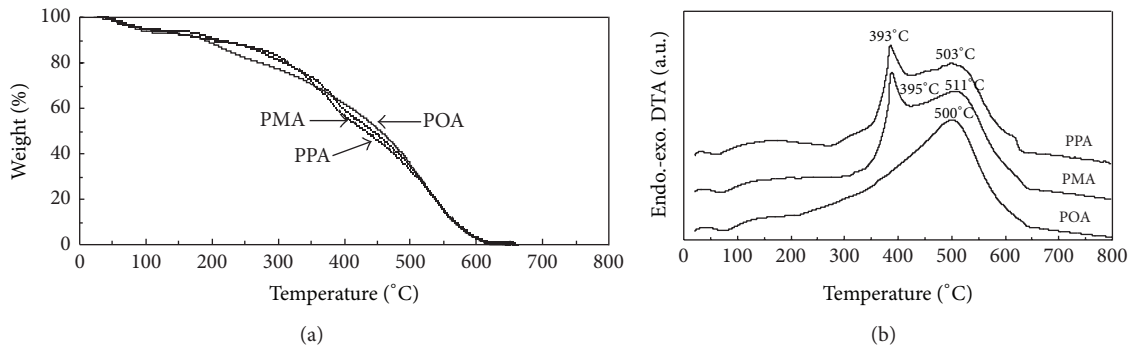

Figure 3: TG curves (a) and DTA curves (b) of polymer POA, PMA, and PPA.

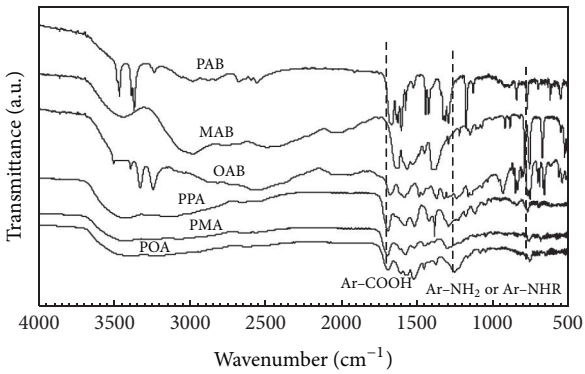

Figure 4: FT-IR spectra of POA, PMA, and PPA polymer samples and OAB, MAB and PAB monomer.

The bands at 823 and 871 cm^{-1} in FTIR spectra of POA are assigned to bend vibration of C–H of aromatic ring occurring 1,2,4-disubstituted. In the chemical structure of POA, whose scheme has been shown in literature 16, the ortho-position (occupied by a nitrogen atom) to one carboxylate group at a given monomeric unit would be located in meta-position relative to the carboxylate group of the neighboring unit. One nitrogen atom is located the para-position to other nitrogen atom on an aromatic ring. In fact, ortho-, meta-, and para-aminobenzoic acids should give polymers with quite the same chemical structure. But there are some differences in their chemical structure. The bands at 837, 867, and 683 cm^{-1} in FTIR spectra of PMA are assigned to bend vibration of C–H of aromatic ring occurring 1,3,5-disubstituted. The result is close to the theoretical analysis since there are the steric effect and the substituent effect. Therefore, in the chemical structure of PMA, one nitrogen atom is located the meta-position to other nitrogen atom on an aromatic ring. The bands at 845 and 871 cm^{-1} in FTIR spectra of PPA are assigned to bend vibration of C–H of aromatic ring occurring 1,2,4-disubstituted. The result agreed with the theoretical analysis by the steric effect and the substituent effect in this synthesis. Therefore, in the structure of polymer PPA, one nitrogen atom is located the ortho-position to other nitrogen atom on an aromatic ring.

3.2. Formation of Polymer/TiO_2 Nanocomposites. Two kinds of typical commercial TiO_2 nanocrystal samples ST01 with a crystal size of about 7 nm and P25 with a crystal size of about 30 nm were used for the preparation of polymer/TiO_2 nanocomposites. The samples ST01 and P25 have a value of BET specific surface area (S_{BET}) as 349, and 63 $m^2 \cdot g^{-1}$ respectively, corresponding to their crystal sizes. Nanocomposite of polymer and TiO_2 nanocrystals can be obtained by adsorbing polymer on the TiO_2 nanocrystal surface. The preparing nanocomposite samples have been measured by specific surface area. These polymer/ST01 and polymer/P25 nanocomposites have a S_{BET} value as 348 and 61 $m^2 \cdot g^{-1}$ for PPA, 341 and 62 $m^2 \cdot g^{-1}$ for PMA, and 344 and 62 $m^2 \cdot g^{-1}$ for POA, respectively. The results indicate the particle size of these nanocomposites is in a nanoscale. Figure 5 showed

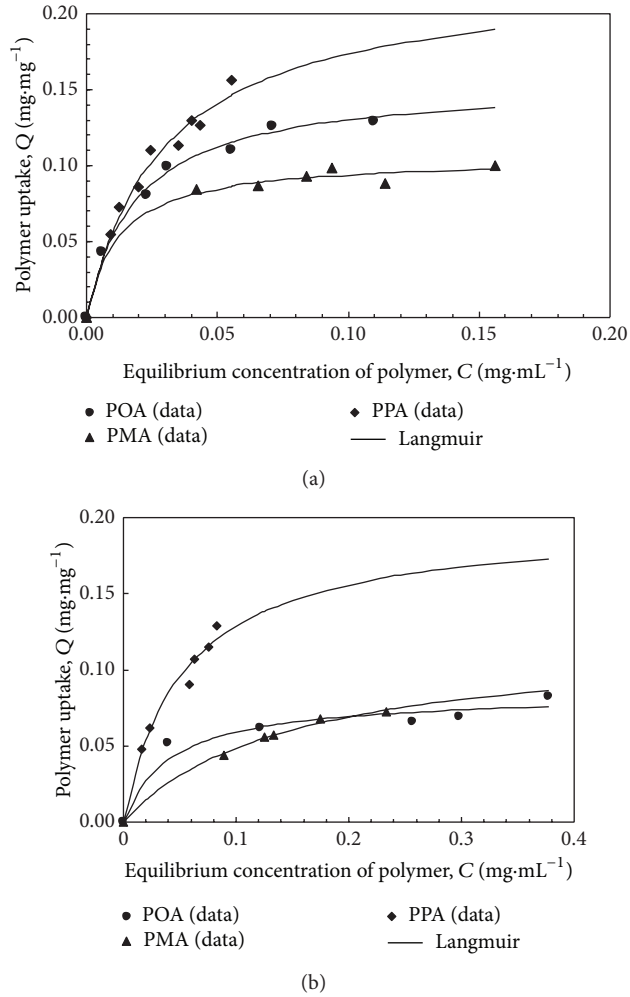

Figure 5: The isotherms for the polymers (concentration range: 0.06 to 0.5 $g \cdot L^{-1}$) adsorption on TiO_2 samples. (a) ST01 and (b) P25.

the adsorption isotherms of synthesized polymers on TiO_2 nanocrystal samples ST01 and P25 at room temperature. The experimental data fit the Langmuir isotherm for all these samples. Thus the adsorptions of PPA, PMA, and POA on the TiO_2 nanocrystals can be explained using the Langmuir monolayer adsorption model [23]. The Langmuir equation can be represented in the linear formula (1):

$$\frac{C}{Q} = \frac{1}{(Q_m K_{ad})} + \frac{C}{Q_m}, \quad (1)$$

where Q is PPA, or PMA or POA uptake ($mg \cdot mg^{-1}$), C is the equilibrium concentration of the polymer in the solution ($mg \cdot mL^{-1}$), Q_m is the saturation (maximum) adsorption capacity ($mg \cdot mg^{-1}$), and K_{ad} is the adsorption constant ($mL \cdot mg^{-1}$). From the fitting of experimental data by plotting C/Q against C, the saturation capacity (Q_m) and the adsorption constant (K_{ad}) for PPA, PMA, and POA adsorptions were evaluated, respectively, and listed in Table 2. The adsorption parameters of dye N719 on TiO_2 nanocrystals sample are also shown in Table 2 for the comparison.

Table 1: The data about UV-visible and FT-IR spectra of the monomers, polymers, and N719 dye.

Sample	Color	UV peak/abs. coef. ($nm/L{\cdot}g^{-1}{\cdot}cm^{-1}$)[a]	Average value of abs. coef. in 400–600 nm ($L{\cdot}g^{-1}{\cdot}cm^{-1}$)	FT-IR vibration band wavenumber (cm^{-1})[b,c]
PAB	Colourless	280, 222		3364 s 3461 m 3053 m 1686 vs 1626 s 1603 vs 1576 s 1523 m 1443 s 1422 s 1351 s 1296 vs 1201 vw 1130 m 1056 vw 1048 vw 920 m 843 m
MAB	Colourless	319, 254		1624 vs 1567 vs 1527 s 1487 sh 1452 s 1390 vs 1325 sh 1293 m 1150 m 1095 w 1072 w 1005 w 919 m 886 m 790 vs 673 s
OAB	Colourless	336, 248, 223		3495 s 3382 vs 3040 1680 vs 1610 vs 1559 vs 1585 vs 1487 s 1460 m 1428 s 1326 s 1241 vs 1164 s 1114 m 1064 w 1026 w 971 w 921 s 764 vs
PPA	Brown	391/24.0, 300/42.7, 206/66.9	9.27	3428 m 3136 m 1692 vs 1638 sh 1629 sh 1579 s 1518 s 1422 m 1385 vs 1344 sh 1292 s 1180 m 1120 m 1155 w 1059 m 1016 w 948 vw 871 w 845 m
PMA	Brown-black	346/28.6, 331/28.7, 221/98.8	6.02	3416 m 3223 m 1697 s 1637 w 1610 sh 1579 s 1516 m 1456 m 1424 w 1385 m 1301 s 1165 w 1108 w 1040 w 1002 vw 915 vw 867 vw 837 w 760 s 683 m
POA	Black	550/7.62, 350/26.0, 215/101.7	9.73	3379 m 3227 m 2611 w 1688 s 1606 s 1567 s 1517 vs 1453 m 1385 m 1247 vs 1167 m 1082 w 1046 w 1003 vw 982 vw 955 vw 756 s 982 vw 871 vw 823 m 756 s
N719	Black	528/5.52, 389/5.42, 311/18.9, 231/16.6	3.74	2964 s 2876 w 2104 vs 1714 s 1611 s 1543 m 1467 m 1437 vw 1406 m 1370 s 1237 s 1149 vw 1021 w

[a]UV-vis absorption measured in ethanol.
[b]sh: shoulder.
[c]vs: very strong; s: strong; m: medium; w: weak; vw: very weak.

Table 2: The adsorption parameters of PPA, PMA, POA, and N719 dyes on TiO_2.

Polymer sample	TiO_2 sample/Phase	S_{BET} ($m^2{\cdot}g^{-1}$)	Saturation adsorption capacity Q_m ($mg{\cdot}mg^{-1}$)/($mg{\cdot}m^{-2}$)	Adsorption constant K_{ad} ($mL{\cdot}mg^{-1}$)	Correlation coefficient r	Data point n
PPA	ST-01/a	349	0.226/0.640	33.4	0.975	9
PMA	ST-01/a	349	0.105/0.301	83.2	0.991	7
POA	ST-01/a	349	0.155/0.444	52.9	0.999	8
N719	ST-01/a	349	0.198/0.594	5.40	0.998	7
PPA	P-25/a + r	63	0.197/3.12	18.8	0.958	7
PMA	P-25/a + r	63	0.120/1.90	6.86	0.989	6
POA	P-25/a + r	63	0.084/1.33	24.0	0.981	6
N719	P-25/a + r	63	0.059/1.19	9.71	0.983	4

It is observed that the majority adsorption constant K_{ad} value for polymers is larger than that for N719, except PMA adsorption on P25. This result suggests the adsorptions of polymers on TiO_2 nanocrystals are stronger than that of N719. The saturation capacity Q_m value (mg/mg (TiO_2)) for polymers is approach or larger than that for N719. The molecular weight of chemical composition corresponding per –COOH group for the polymers is much smaller than that of N719. If the Q_m value is in M(–COOH)/mg (TiO_2) unit, where M(–COOH) is amount (mole) of –COOH group adsorbed on TiO_2, the Q_m value (mmole/g (TiO_2)) of polymers are much larger than that of N719.

It has reported that the carboxylic acid or carboxylate groups of organic molecules can coordinate to the TiO_2 surface by various bonding modes, such as (a) unidentate mode, (b) chelating mode (4-membered bidentate), and (c) bidentate bridging mode [24–26]. Since the asymmetric and symmetric IR absorptive bands of carboxylate groups are different each other in these binding modes, these modes can be identified by the IR spectrum data. It has been reported that if the wavenumber difference between the asymmetric and symmetric bands in the adsorbed state is lower than that in the free-state, then the anchoring mode is bidentate chelating or bidentate bridging, while if the wavenumber difference is greater or equal to that in the free-state, then anchoring mode is unidentate [27].

Figure 6 showed the FT-IR spectra of the nanocomposite samples obtained by adsorbing PPA, PMA, and POA on

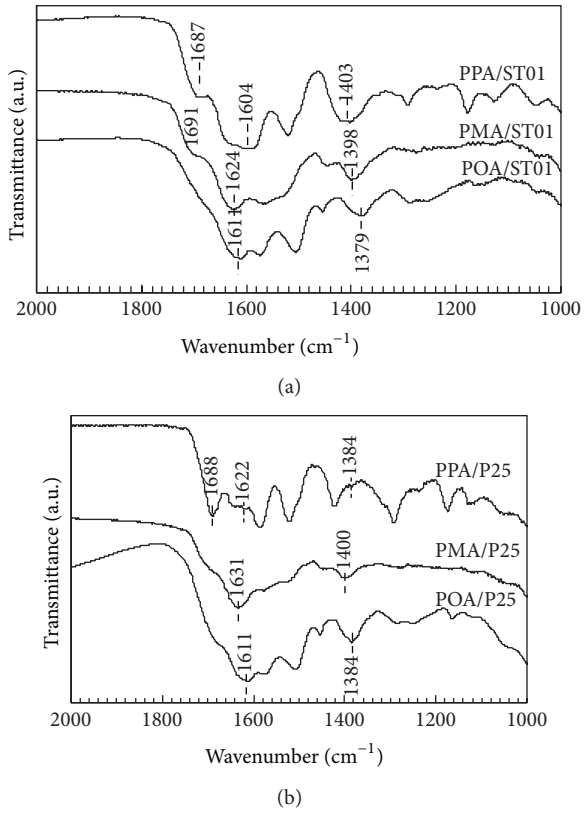

Figure 6: FT-IR spectra of POA/TiO_2, PMA/TiO_2, and PPA/TiO_2 nanocomposite samples. (a) ST01 and (b) P25.

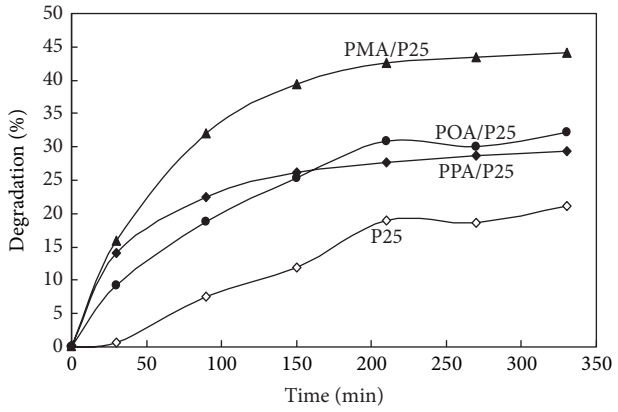

Figure 7: Changes of degradation ratio of methylene blue with irradiation time for PMA/P25, POA/P25, and PPA/P25 nanocomposite samples and P25 under the incandescent lamp irradiating conditions.

the TiO_2 nanocrystal surface. The intensities of ν(C=O) and ν(C–OH) bands of carboxylic acid groups (–COOH) decreased largely after being adsorbed on TiO_2 for PPA, PMA, and POA, and the decreased intensity is follow as PPA > PMA > POA. The result reveals –COOH groups were deprotonated to $–COO^-$ groups after the adsorptions, and the order of deprotonated degree in accord with that of the decreased intensity. As shown in Figures 4 and 6, the wavenumber differences between the carboxylate group asymmetric and symmetric bands of POA, PPA and PMA in the free state are 221, 194 and 225 cm^{-1}, and that in adsorbed state are 232, 201 and 227 cm^{-1}, respectively, for the polymer/ST01 nanocomposite sample. The wavenumber differences are larger than that in the free-state, and the results are identical for the polymer/P25 nanocomposite sample. The results suggest that the polymers anchor as unidentate coordination to the TiO_2. It has been reported that the carboxylate groups in N719 anchor to the TiO_2 surface with bidentate chelating or bridging binding mode [16, 20]. Although the bidentate chelating and bridging binding modes are more stable than the unidentate mode, meaning that the adsorption of N719 must be more stable than that of the polymers. But the adsorption isotherm results revealed that adsorption constant (K_{ad}) of the polymers is larger than that of N719 (Table 2). This fact can be explained by formation of a multibridging chelating mode in the polymer/TiO_2 nanocomposite [16]. Each polymer molecule has many carboxylate groups, and each carboxylate group can coordinate to TiO_2 surface with the unidentate mode, which forms the multi-bridging chelating mode, and enhances the stability of the adsorption.

3.3. Activities of Polymer/TiO_2 Nanocomposites in Visible Photocatalytic Reaction. The nanocomposites prepared by adsorbing polymer on surface of P25 or ST01 nanoparticles were employed in visible photocatalytic degradation of methylene blue (MB) to measure their visible photocatalytic activities. Figure 7 showed the changes of the degradation ratio of MB with photocatalytic reaction time for POA/P25, PMA/P25 and PPA/P25 nanocomposite samples and P25 under the incandescent lamp irradiating conditions. The results showed the degradation ratio of MB at 330 min as 44.1%, 32.2%, 29.3%, and 21.1% for PMA/P25, POA/P25, PPA/P25, and no sensitized P25, respectively. The PMA/P25 nanocomposite showed the highest degradation rate in all testing samples. And that for all polymer/P25 nanocomposite samples is higher than the polymer-free P25 sample under visible light irradiating conditions. Furthermore, the photocatalytic degradation process was studied on the dynamics. The related data are summarized in Table 3. It can be found that these reactions are first order reaction and the reaction rate is proportional to the concentration of MB. The rate constant k increased according to the sequence of P25 < POA/P25 < PMA/P25 < PPA/P25, indicating the reaction activation energy of the order of decreasing, therefore, the catalytic activity of the catalysts is enhanced in this order. These results indicate the visible light sensitizing effect of PPA, PMA, and POA on TiO_2 nanocrystal surface for the photocatalytic reaction.

Figure 8 showed UV-visible spectra of MB solution degraded for the polymer/ST01 and N719/ST01 nanocomposites samples under indoors-light irradiating conditions for 3d. It is found that the visible photocatalytic activity of POA/ST01 sample is higher than that of others. The result showed the degradation ratio of MB at 3d as 77.5%, 66.3%, 47.2%, 22.3%, and 16.1% for POA/ST01, PMA/ST01, PPA/ST01, N719/ST01,

Table 3: The kinetic data about the photocatalytic reactions degrading methylene blue for PMA/P25, POA/P25 and PPA/P25 nanocomposite samples and P25 under the incandescent lamp irradiating conditions.

Sample	Rate constant k (min^{-1})	Kinetic equation, $v = kc + A$	Reaction order	Correlation coefficient r	Data point n
PPA/P25	0.0037	$v = 0.0037c - 0.0391$	1	0.999	6
PMA/P25	0.0020	$v = 0.0020c - 0.0136$	1	0.983	6
POA/P25	0.0014	$v = 0.0013c - 0.0120$	1	0.997	5
P25	0.0002	$v = 0.0002c - 0.0012$	1	0.996	5

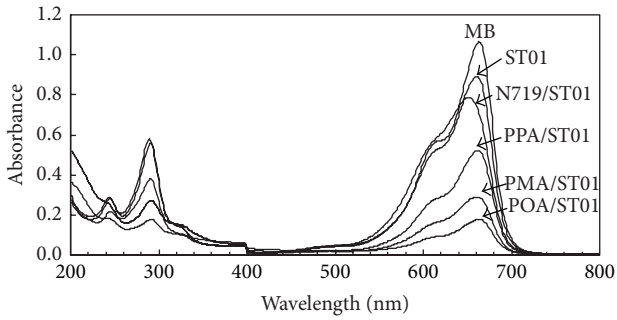

Figure 8: UV-visible spectra of methylene blue solution degraded for ST01 sensitized by the polymers and dye N719 under indoors-light irradiating conditions for 3d.

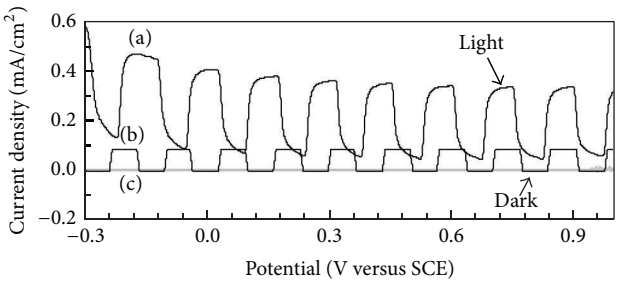

Figure 9: Current-voltage curves of (a) PPA/ST01 film, (b) PMA/ST01 film, and (c) ST01 nanocrystalline film in aqueous solution containing 0.1 mol/L of sodium sulfate in the dark and under irradiation with light (400–700 nm).

and no sensitized ST01, respectively. This result suggests that samples from POA and PMA have strong adsorbing character and higher visible photocatalytic activity than that of others. And the syntactic polymer/ST01 samples used as a photocatalyst have more advantages than N719/ST01 sample in visible photocatalytic activity, synthesis condition and producing cost.

The visible photocatalytic activity of the polymer/TiO_2 nanocomposite is further demonstrated by the results of photoelectrochemical study. Figure 9(a) is a typical current-voltage curve obtained by irradiating intermittently the PPA/ST01 nanocomposite film electrode with a 100 W Xe lamp with 400–700 nm wavelengths. When the potential was scanned from −0.3 to 1.2 V (versus SCE), the photocurrent decreased slightly with increasing the applied potential, and so for the dark current, which is due to electrochemical

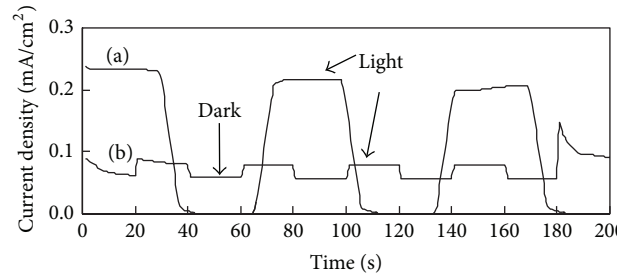

Figure 10: Current-time curves of (a) PPA/ST01 film (applied pressure E = 0 mV) and (b) POA/ST01 film (applied pressure E = 200 mV) in aqueous solution containing 0.1 mol/L of sodium sulfate in the dark and under irradiation with light (400–700 nm).

oxidation reaction of PPA on the electrode [22]. The hydrogen gas evolution was observed at the Pt counter electrode accompanying the photocurrent, suggesting the reduction of H^+ to H_2. Figure 9(b) is a typical current-voltage curve obtained at the same conditions for PMA/ST01 nanocomposite. It is observed that the almost constant photocurrent is much lower than that of PPA/ST01 nanocomposite, and the dark current closed to zero. The polymer-free ST01 film was also employed for the comparison, but without photocurrent was observed in the current-voltage curve under the same conditions (Figure 9(c)). The results indicate PPA/ST01 and PMA/ST01 nanocomposites are the material with visible photoelectrochemical activity, and the activity of PPA/ST01 nanocomposites is more than three times PMA/ST01 in the photocatalytic reaction.

Figure 10 showed current-time curves of PPA/ST01 film at zero applied pressure (Figure 10(a)) and POA/ST01 film when applied pressure E is 200 mV (Figure 10(b)) in aqueous solution containing 0.1 mol/L of sodium sulfate in the dark and under irradiation with light (400–700 nm). It is observed that the photocurrent for PPA/ST01 film is still much higher than that at applied pressure as 200 mV for POA/ST01 film although the applied pressure closes zero. The above results suggest that visible photoelectrochemical activity of PPA/ST01 nanocomposites is the highest among the three.

4. Conclusions

Three kinds of poly(aminobenzoic acid) were synthesized by oxidizing *p*-, *m*-, or *o*-aminobenzoic acid with an oxidizing agent of peroxodisulfate ammonium in an acidic solution. The influences produced by the amount of oxidizing agent

and the acid are different in the synthesis of PPA, PMA, and POA because of the difference of site of amino group in aminobenzoic acid. The polymer/TiO_2 nanocomposite can be obtained by adsorbing the polymer on TiO_2 surface and shows high stability, due to that the carboxylate groups anchor to the TiO_2 surface with the multi-bridging chelating mode. PMA/P25 and PPA/ST01 nanocomposites exhibit much higher visible photocatalytic activity than others in the photocatalytic reaction, and PPA/ST01 nanocomposite reveals higher visible photoelectrochemical activity than others. Therefore, they have a potential application as visible light photocatalyst.

Acknowledgments

This work was supported by the Grants-in-Aid for the Natural Science Foundation of China (no. 21173003), the Scientific Research Project (no. 2011JM2009) from Science and Technology Department of Shaanxi Province, and Key Research Project (no. ZK1051) from Baoji University of Arts and Sciences.

References

[1] H. Kominami, S.-Y. Murakami, J.-I. Kato, Y. Kera, and B. Ohtani, "Correlation between some physical properties of titanium dioxide particles and their photocatalytic activity for some probe reactions in aqueous systems," *The Journal of Physical Chemistry B*, vol. 106, no. 40, pp. 10501–10507, 2002.

[2] I. Nakamura, N. Negishi, S. Kutsuna, T. Ihara, S. Sugihara, and K. Takeuchi, "Role of oxygen vacancy in the plasma-treated TiO_2 photocatalyst with visible light activity for NO removal," *Journal of Molecular Catalysis A*, vol. 161, no. 1-2, pp. 205–212, 2000.

[3] H. Irie, Y. Watanabe, and K. Hashimoto, "Nitrogen-concentration dependence on photocatalytic activity of $TiO_{2-x}N_x$ powders," *The Journal of Physical Chemistry B*, vol. 107, no. 23, pp. 5483–5486, 2003.

[4] E. Borgarello, J. Kiwi, M. Grätzel, E. Pelizzetti, and M. Visca, "Visible light induced water cleavage in colloidal solutions of chromium-doped titanium dioxide particles," *Journal of the American Chemical Society*, vol. 104, no. 11, pp. 2996–3002, 1982.

[5] T. Yoshida, T. Tanaka, T. Yamamoto, S. Yoshida, H. Ishitani, and S. Kobayashi, "XAFS study of ytterbium complexes as new-type Lewis acid catalysts," *Journal of Synchrotron Radiation*, vol. 6, no. 3, pp. 455–457, 1999.

[6] M. Grätzel, "The artificial leaf, molecular photovoltaics achieve efficient generation of electricity from sunlight," *Comments on Inorganic Chemistry*, vol. 12, no. 2-3, pp. 93–111, 1991.

[7] P. Péchy, F. P. Rotzinger, M. K. Nazeeruddin et al., "Preparation of phosphonated polypyridyl ligands to anchor transition-metal complexes on oxide surfaces: application for the conversion of light to electricity with nanocrystalline TiO_2 films," *Journal of the Chemical Society*, no. 1, pp. 65–66, 1995.

[8] A. Kay and M. Grätzel, "Photosensitization of titania solar cells with chlorophyll derivatives and related natural porphyrins," *The Journal of Physical Chemistry*, vol. 97, no. 23, pp. 6272–6277, 1993.

[9] K. Sayama, K. Hara, N. Mori et al., "Photosensitization of a porous TiO_2 electrode with merocyanine dyes containing a carboxyl group and a long alkyl chain," *Chemical Communications*, no. 13, pp. 1173–1174, 2000.

[10] Z.-S. Wang, F.-Y. Li, and C.-H. Huang, "Photocurrent enhancement of hemicyanine dyes containing RSO_3^- group through treating TiO_2 films with hydrochloric acid," *The Journal of Physical Chemistry B*, vol. 105, no. 38, pp. 9210–9217, 2001.

[11] K. Hara, M. Kurashige, Y. Dan-oh et al., "Design of new coumarin dyes having thiophene moieties for highly efficient organic-dye-sensitized solar cells," *New Journal of Chemistry*, vol. 27, no. 5, pp. 783–785, 2003.

[12] M. Dürr, A. Bamedi, A. Yasuda, and G. Nelles, "Tandem dye-sensitized solar cell for improved power conversion efficiencies," *Applied Physics Letters*, vol. 84, no. 17, pp. 3397–3399, 2004.

[13] Y. N. Xia, J. M. Wiesinger, A. G. MacDiarmid, and A. J. Epstein, "Camphorsulfonic acid fully doped polyaniline emeraldine salt: conformations in different solvents studied by an ultraviolet/visible/near-infrared spectroscopic method," *Chemistry of Materials*, vol. 7, no. 3, pp. 443–445, 1995.

[14] J. Huang, S. Virji, B. H. Weiller, and R. B. Kaner, "Polyaniline nanofibers: facile synthesis and chemical sensors," *Journal of the American Chemical Society*, vol. 125, no. 2, pp. 314–315, 2003.

[15] E. Westerweele, P. Smith, and A. J. Heeger, "'Inverted' polymer light-emitting diodes on cylindrical metal substrates," *Advanced Materials*, vol. 7, no. 9, pp. 788–790, 1995.

[16] P. Wen, S. Yang, Y. Ishikawa, H. Itoh, and Q. Feng, "Visible light sensitization effect of polyaminobenzoate adsorbed on TiO_2 nanocrystal surface," *Applied Surface Science*, vol. 257, no. 6, pp. 2126–2133, 2011.

[17] M. Adachi, Y. Murata, J. Takao, J. Jiu, M. Sakamoto, and F. Wang, "Highly efficient dye-sensitized solar cells with a titania thin-film electrode composed of a network structure of single-crystal-like TiO_2 nanowires made by the "oriented attachment" mechanism," *Journal of the American Chemical Society*, vol. 126, no. 45, pp. 14943–14949, 2004.

[18] X.-L. Wei, Y. Z. Wang, S. M. Long, C. Bobeczko, and A. J. Epstein, "Synthesis and physical properties of highly sulfonated polyaniline," *Journal of the American Chemical Society*, vol. 118, no. 11, pp. 2545–2555, 1996.

[19] W. Li and H.-L. Wang, "Oligomer-assisted synthesis of chiral polyaniline nanofibers," *Journal of the American Chemical Society*, vol. 126, no. 8, pp. 2278–2279, 2004.

[20] M. K. Nazeeruddin, R. Humphry-Baker, P. Liska, and M. Grätzel, "Investigation of sensitizer adsorption and the influence of protons on current and voltage of a dye-sensitized nanocrystalline TiO_2 solar cell," *The Journal of Physical Chemistry B*, vol. 107, no. 34, pp. 8981–8987, 2003.

[21] W. Liu, J. Kumar, S. Tripathy, K. J. Senecal, and L. Samuelson, "Enzymatically synthesized conducting polyaniline," *Journal of the American Chemical Society*, vol. 121, no. 1, pp. 71–78, 1999.

[22] M. Samsonowicz, T. Hrynaszkiewicz, R. Świsłocka, E. Regulska, and W. Lewandowski, "Experimental and theoretical IR, Raman, NMR spectra of 2-, 3- and 4-aminobenzoic acids," *Journal of Molecular Structure*, vol. 744–747, pp. 345–352, 2005.

[23] M. Xue, R. Chitrakar, K. Sakane et al., "Selective adsorption of thiophene and 1-benzothiophene on metal-ion-exchanged zeolites in organic medium," *Journal of Colloid and Interface Science*, vol. 285, no. 2, pp. 487–492, 2005.

[24] A. Islam, H. Sugihara, and H. Arakawa, "Molecular design of ruthenium(II) polypyridyl photosensitizers for efficient

nanocrystalline TiO_2 solar cells," *Journal of Photochemistry and Photobiology A*, vol. 158, no. 2-3, pp. 131–138, 2003.

[25] T. Ma, K. Inoue, H. Noma, K. Yao, and E. Abe, "Effect of functional group on photochemical properties and photosensitization of TiO_2 electrode sensitized by porphyrin derivatives," *Journal of Photochemistry and Photobiology A*, vol. 152, no. 1–3, pp. 207–212, 2002.

[26] A. Vittadini, A. Selloni, F. P. Rotzinger, and M. Grätzel, "Formic acid adsorption on dry and hydrated TiO_2 anatase (101) surfaces by DFT calculations," *The Journal of Physical Chemistry B*, vol. 104, no. 6, pp. 1300–1306, 2000.

[27] G. B. Deacon and R. Phillips, "Relationships between the carbon-oxygen stretching frequencies of carboxylato complexes and the type of carboxylate coordination," *Coordination Chemistry Reviews*, vol. 33, no. 3, pp. 227–250, 1980.